Evaluation of the use of ceramic foams as catalyst supports for reverse-flow combustors

Claire R. Thompson, Pablo Marín, Fernando V. Díez, Salvador Ordóñez*

Department of Chemical Engineering and Environmental Technology, University of Oviedo, Facultad de Química, Julián Clavería 8, Oviedo 33006, SPAIN

* Phone: 34-985 103 437, FAX: 34-985 103 434, e-mail: sordonez@uniovi.es

Abstract

The performance of a silicon carbide foam supported palladium catalyst (Pd/β-SiC) in a reverse flow reactor for the abatement of methane in diluted streams (2700-5400 ppm) has been studied in this article. The limits of stable operation for this configuration have been experimentally established, being narrower than the corresponding to particulated and honeycomb monolith beds because of the lower thermal inertial of foamed beds. A heterogeneous one-dimensional model has been developed (including the use of specific correlations for mass transfer and dispersive terms) and experimentally validated for predicting the behavior of these reactors.

Finally, the numerical model has been used for simulating reverse-flow reactors equipped with different catalyst shapes (e.g. Raschig rings, honeycomb monoliths and foams) of equivalent geometry. Results for different superficial velocities (0.25-1.5 m/s) are compared in terms of transport properties and performance, concluding that honeycomb monolithic beds are the most appropriate configuration for these devices.

Keywords: cellular foam; silicon carbide; afterburner; lean fuel; dynamic modelling; methane catalytic combustion; reverse flow reactors.

1. Introduction

Reverse-flow catalytic combustors consist of a catalytic fixed bed, where the feed flow direction is periodically reversed. This device is very appropriate for the combustion of lean hydrocarbon/air mixtures because, if operated adequately, most of the heat released by the reaction during one cycle is stored in the solid bed and used to pre-heat the feed in the following cycle. The high thermal efficiency attained allows working at autothermal conditions even for feeds at low temperature with very low hydrocarbon concentration [1, 2].

Reverse-flow catalytic combustors have been applied to the complete oxidation of hydrocarbon pollutants at very low concentrations (100-3000 ppm) [2, 3]. Methane is considered the hydrocarbon most difficult to oxidize, requiring the highest temperature, even in presence of catalysts. For this reason, in this work, methane has been chosen as model compound to test the performance of the catalytic reverse-flow technology. In addition, methane emissions, mainly originated in landfills, coal mining, and natural gas extraction and distribution, constitute an important environmental problem. Methane is a greenhouse gas more than twenty times more powerful than carbon dioxide, so its oxidation to carbon dioxide reduces greatly the net greenhouse gas emissions and contributes to mitigate the global warming [4, 5].

The selection of the type of bed is of great importance in the design of reverse-flow catalytic reactors. Beds formed by random particles lead to important pressure drops, which is not practical when the gas flow rate is high. On the contrary, structured beds (e.g. honeycomb monoliths or foams) exhibit very low pressure drops, and for this reason the interest of this type of bed has raised in the last years. However, the operation with these configurations is problematic because of their poorer mass transfer and their lower thermal inertial.

Cellular foams consist of a reticulated 3D structure with high porosity and surface area, typically made of ceramic (alumina, silicon carbide, cordierite, etc.) or metallic materials (copper, aluminium, etc.). Cellular foams are used in high performance heat exchangers, energy absorbers, thermal insulators, high temperature filters for molten metals, gas filters, etc. [6, 7]. Recently, cellular foams have been proposed as structured catalyst supports, as they can improve heat and mass transfer with respect to more conventional structured supports, such as honeycomb monoliths. Thus, the intricate pore network of the foam creates turbulence in the fluid that continually breaks the hydrodynamic boundary layer, resulting in higher mass and heat transfer coefficients than for honeycomb monolith supports, where the flow pattern is usually laminar. Foam supports share with honeycomb monoliths the low pressure drop and high bed porosity, which allow reactor operation at very high superficial velocities (high flow rates) [5, 8].

Silicon carbide foams crystallized as the cubic structure (β-SiC) are especially suiteable as catalyst supports for high temperature and exothermic reactions. This material presents high thermal and chemical resistance, thermal conductivity, thermal shock resistance, and mechanical strength, as studied by different authors [9, 10]. These properties can lead to important improvements with respect to conventional supports used in catalytic combustion, and particularly reverse-flow reactors, where the movement of the high temperature plateau along the reactor requires a bed material with high thermal shock resistance. Although the surface area of β-SiC (15-25 m^2/g) is far lower than for other supports such as alumina (220 m^2/g) or silica (200 m^2/g), it is similar to that of other high thermal resistance supports, e.g. zirconia (15-30 m^2/g) and much larger than that of α-SiC foams (1 m^2/g) [11]. This means that β-SiC foams can be used directly as catalyst support without the need of a washcoating with high specific surface area. This reduces considerably the complexity of the catalyst manufacture and hence the cost of the catalyst [12].

The complexity of the foam reticulated structure makes the correlation of the transport properties more difficult than for other structured materials (e.g. honeycomb monoliths, wires, etc.), as pointed out in the few works published on this topic in the last years. Pressure drop has been deeply studied in previous works, as reviewed by Edouard at al. [13]. Mass and heat transfer have also been studied by different authors under a wide range of operating conditions [6, 14-17]. The works regarding reaction studies are scarcer, and mainly focused on catalytic oxidations [18-20] and porous media burners [21, 22].

Reverse-flow reactors equipped with random particle beds have been the most studied [1, 2, 23, 24], followed by honeycomb monolith bed [8, 25, 26], while very little attention has been paid to foam beds. The present work aims to fill this gap, by studying experimentally the performance of foam beds in reverse-flow reactors for the catalytic combustion of very lean methane/air mixtures using a Pd/β-SiC foam catalyst, prepared and tested as methane combustion catalyst in a previous work [27].

The aim of this work is to investigate the viability of foam beds as catalyst supports in reverse flow reactors. First, experiments were carried out in a bench-scale reverse-flow reactor varying the the most important operating variables (methane inlet concentration, switching time and gas flow rate), so that to study their influence in the long-term stability of the reactor. Secondly, the experiments are used to validate a mathematical model for reverse-flow reactors with correlations especially suited for foam beds. Finally, the model is used to compare the performance of random particle, honeycomb monolith and ceramic foam beds. The comparison is carried out for catalytic beds with the same Pd loading, washcoating thickness and specific surface area. For each bed type, an industrial-scale reverse-flow reactor is designed to achieve 99% methane conversion. Then, the performance of the designs is compare in terms of reactor size, pressure drop, reactor temperature and related to geometric and transport properties.

2. Methodology

2.1. Catalyst preparation

The foam support consists of β-SiC foam cylindrical blocks, supplied by SICAT. This material presents medium specific surface area (25 m^2/g), making unnecessary the addition of a porous washcoat layer. Palladium was selected as active phase for the catalyst, since it is widely accepted that is the most active metal for methane combustion [28]. Pd was introduced on the β-SiC support by dry impregnation (incipient wetness) with a 0.62 mol/L $Pd(NO_3)_2$ aqueous solution, followed by drying (110ºC, overnight), and calcination (550ºC, 2h). The resulting catalyst has a Pd loading of 2% (w/w). In a former work [27], this catalyst was prepared and tested for methane combustion, ground to small particles, in a laboratory-scale reactor. It was concluded that this catalyst was stable upon time at reaction conditions, and different intrinsic kinetic models were fitted to the experimental results.

2.2. Catalyst characterization

The foam catalyst has been characterized using different techniques. The foam geometry was measured directly using the images from a stereomicroscope (Stemi 2000, ZEISS). As indicated in Figure 1, the basic geometrical properties of foams are: cell size (ϕ), pore size (a) and strut thickness (d_s). Using these basic geometries, and a suitable cell model [29], other geometrical foam properties, such as cell density (ppi), porosity (ε_b) or specific external surface area (S_v), can be derived. The values shown in Table 1 are the average measured for 12 different cells of the foam.

Textural characteristics (specific internal surface area and pore volume) were measured by nitrogen adsorption at 77 K in a Micromeritics ASAP 2020 surface area analyzer. The pore size distribution obtained is mono-modal, corresponding to a large-pore mesoporous structure

(Table 1). Further details on the preparation, characterization, and stability at reaction conditions of the Pd/β-SiC catalyst can be found in [27].

2.3. Experimental device

The bench-scale reverse-flow reactor used in the present work consists of a 0.8 m long 0.05 m internal diameter 316 stainless steel tube. This tube houses three foam beds: one catalytic (0.25 m long) situated in the middle, and two inert (0.125 m long each) situated at both ends. The beds are surrounded by a glass wool layer, in order to avoid gas bypass near the reactor wall. The temperature of the bed is measured in 7 points along the reactor axis using a multipoint thermocouple array. The flow reversal is accomplished by using two pairs of solenoid valves (Parker-Lucifer 121K46E), acting on the reactor inlet and outlet streams. Reactor feed, consisting of methane-air mixture with different methane concentrations, is set using two mass flowmeters (Bronkhorst F201C). The analysis of methane concentration at the inlet and outlet streams is performed continuously (each 5 seconds) using an infrared spectrometer (ABB- PIR3502).

The reactor tube is surrounded by an oven, equipped with a dynamic temperature-control system able of compensating the heat transfer through the reactor tube, and hence allowing a reactor operation close to adiabatic. The working principle has been explained in more detail and the behavior of this unit demonstrated in previous works [23, 30]. The near-adiabatic operation of this unit is very difficult to accomplish for bench-scale and smaller units, with high external surface/volume ratio, and it resembles the behavior of industrial-scale reverse-flow reactors, usually of large diameter and hence with low external surface/volume ratio, which tend to be intrinsically adiabatic.

The following protocol has been followed for each test. First, the reactor was fed with hot air (400ºC) in order to pre-heat the beds above the ignition temperature of the air-methane mixture. Then, the selectedmethane/air mixture was fed to the reactor at room temperature (20ºC) and the flow reversal was started. If the cycle time (the time elapsed between two consecutive valve switches) is low enough, the heat of combustion trapped in the reactor bed during one cycle is enough to pre-heat the cold feed in the following cycle and the reactor is self-sustained (autothermal behaviour). In this situation, a pseudo-steady state will be achieved after a few cycles, in which the evolution of temperature and concentration profiles is exactly repeated in all the consecutive cycles. Otherwise, the temperature of the reactor decreases gradually cycle after cycle, and finally the reactor extinction takes place.

2.4. Reactor model

Many different types of models have been proposed to relate operating and design variables in reverse-flow reactors, the most popular being those that predict directly the evolution of the reactor temperature and concentration profiles at unsteady state [31]. These models, though are the most complex, can provide accurate predictions of the reactor performance, and for this reason are selected in the present work.

The foam fixed-bed has been modelled using a continuous heterogeneous model. This type of model, unlike pseudo-homogeneous models, accounts explicitly for the gas and solid phases, but does not consider the exact shape of both phases, as in Computational Fluid Dynamic (CFD) models. Continuous heterogeneous models are easier to solve than CFD models, and for this reason are widely used for the simulation of fixed-bed reactors. Our model considers the reactor as adiabatic (as large commercial reactors and our experimental unit), so no radial

gradients are present, and it is only necessary to consider one space dimension: the axial coordinate.

The following set of partial differential equations corresponds to the resulting heterogeneous 1D dynamic model. The equations are conservation equations, eq. (1), applied separately to the gas and solid phases. The meaning of the symbols is indicated in the list of symbols.

(Accumulation) = (Convection) + (Dispersion) + (Interphase transfer) + (Reaction) (1)

Mass balance to the gas phase:

$$\frac{\partial y_{Gj}}{\partial t} = -v_0 \frac{\rho_{G0}}{\rho_G} \frac{\partial y_{Gj}}{\partial z} + D_{j,ax} \frac{\partial^2 y_{Gj}}{\partial z^2} - a_G K_{Gj}\left(y_{Gj} - y_{Sj}\right), \qquad j = CH_4 \tag{2}$$

Mass balance to the solid phase:

$$\frac{\partial y_{Sj}}{\partial t} = a_S K_{Gj}\left(y_{Gj} - y_{Sj}\right) + \frac{\eta_j \rho_{cat} \left(r_j\right)_m}{c_G}, \qquad j = CH_4 \tag{3}$$

Energy balance to the gas phase:

$$\frac{\partial T_G}{\partial t} = -v_0 \frac{\rho_{G0}}{\rho_G} \frac{\partial T_G}{\partial z} + \frac{\kappa_{G,ax}}{\rho_G C_{PG}} \frac{\partial^2 T_G}{\partial z^2} + \frac{a_G h}{\rho_G C_{PG}} \left(T_S - T_G\right) \tag{4}$$

Energy balance to the solid phase:

$$\frac{\partial T_S}{\partial t} = \frac{k_S}{\rho_S C_{PS}} \frac{\partial^2 T_S}{\partial z^2} + \frac{a_S h}{\rho_S C_{PS}} \left(T_G - T_S\right) + \frac{\sum_{j=1}^{C} \eta_j \rho_{cat} \left(r_j\right)_m \Delta H_j}{\rho_S C_{PS}} \tag{5}$$

The physical and transport properties of the gas and solid phase appearing in eq. (2) to (5) must be determined. Transport properties are tightly linked to the type of bed (random particles, honeycomb monolith or foam), and they must be estimated using appropriate correlations. Beds formed by random particles and honeycomb monoliths have been deeply studied, and there are many correlations for them available in the literature [8, 32]. On the contrary, foams have been proposed as catalyst supports very recently, so the number of works regarding transport properties is much lower, and currently there is a lack of generalized accepted correlations, valid for foams of different materials, geometries and sizes. In this work, we collected correlations from the literature, and then selected the one that best matches to our foam (type and geometry).

Gas to solid mass and heat transport coefficients have been estimated using the correlation proposed by Groppi et al. [33], Table 2, who studied metallic and ceramic foams of different sizes (5-15 ppi) at a wide range of operating conditions (Re_{max} = 15-200). They correlated the transport properties using the Reynolds number evaluated at the maximum interstitial velocity (v_{max}), which can be calculated by:

$$v_{max} = v\left(\frac{a}{a-d_s}\right)^2 = \frac{v}{\left[1-\frac{2\sqrt{1-\epsilon_b}}{\sqrt{3\pi}}\right]^2} \quad (2)$$

Another important bed property is the axial dispersion. In foam beds the gas flow is forced through an intricate pore network, which continually breaks the hydrodynamic boundary layer, favouring gas to solid mass and heat transfer, but also axial dispersion. For this reason, and depending on the operating conditions (e.g. superficial velocity), deviations from ideal plug flow are expected, that are characterized by the dispersion terms in eq. (2) to (5). Heat axial dispersion coefficient has been recently measured and correlated by Dietrich et al. [34], Table 2, for 3 ceramic foams with sizes 10-45 ppi. Mass axial dispersion coefficient has been

calculated using the Chilton-Colburn analogy between heat and mass transfer, as shown in Table 2.

Pressure drop in the reactor can be evaluated solving the mechanical energy balance, eq. (7), where the friction factor (*f*) depends on the type of bed. In the last years, several works have been published proposing correlations to determine pressure drops or friction factors as a function of foam geometry, as summarized by Edouard et al. [13]. Here, the expression proposed by Lacroix et al. [7] has been used, as indicated in Table 2.

$$\frac{\partial p}{\partial z} = -\frac{(\rho_{G0} u_0)^2 f}{2\, d\, \rho_G}, \qquad p|_{z=0} = p_0 \tag{3}$$

Regarding the reaction terms of eq. (2) to (5), homogenous reaction in the gas phase has been neglected, because thermal methane oxidation requires a much higher temperature than the catalytic one. The kinetics of the heterogeneous reaction with the Pd/β-SiC catalyst was studied in a laboratory isothermal fixed-bed reactor filled with the catalyst grinded to 300 μm particle size, so that the influence of mass and heat transport processes was negligible, as reported in [27]. The experimental results were fitted to first-order kinetics, $(r_j)_m = k_m p_j$, with the kinetic constant depending on the temperature according to the Arrhenius equation, $k_m = k_0 \exp(-E_a/R_g T)$. The value of the kinetic parameters is shown in Table 1.

The influence of mass transfer inside the pores of the solid foam has been accounted for using the effectiveness factor and Thiele modulus for first-order kinetics at rectangular coordinates, eqs. (8) and (9).

$$\eta_j = \frac{\tanh \phi_j}{\phi_j} \tag{4}$$

$$\phi_j = L_w \sqrt{\frac{k_m \rho_S R_g T_S}{f_w D_{ep}}} \qquad (5)$$

It should be noted that, in most structured catalysts, reaction takes place only in a thin layer of the porous washcoating, and for this reason the kinetic constant obtained for the grinded catalyst, when used for structured catalysts, must be divided by the volume fraction of washcoating (f_W) [8]. In the present work, as our catalyst is a porous β-SiC foam without washcoating, and all the support has been impregnated with active phase, f_W in eq. (9) equals 1. For the same reason, the characteristic length for internal transport (L_w) of the foam has been taken as half the strut diameter. The effective pore diffusion coefficient (D_{ep}) has been determined considering molecular and Knudsen mechanisms [27], and using the textural properties in Table 1.

The resolution of the set of partial differential equations (2) to (5) requires appropriate initial and boundary conditions. As shown in eq. (10) to (14), Danckwerts boundary conditions have been used to account for the dispersion at the reactor inlet. The switch of the feed direction is modeled by shifting the boundary conditions at both sides of the reactor.

Initial conditions:

$$y_G|_{t=0} = y_S|_{t=0} = 0, \qquad T_G|_{t=0} = T_S|_{t=0} = T_{ph} \qquad (10)$$

Boundary conditions:

$$(y_{Gj})_{0^-} = (y_{Gj})_{0^+} - \frac{D_{ax}}{v_0}\left(\frac{\partial y_{Gj}}{\partial z}\right)_{0^+}, \qquad \left(\frac{\partial y_{Sj}}{\partial z}\right)_{z=0^+} = 0 \qquad (11)$$

$$(T_G)_{0^-} = (T_G)_{0^+} - \frac{\kappa_{G,ax}}{v_0 \rho_{G0} C_{PG}} \left(\frac{\partial T_G}{\partial z}\right)_{0^+}, \qquad \left(\frac{\partial T_S}{\partial z}\right)_{z=0^+} = 0 \tag{12}$$

$$p|_{z=0} = p_0 \tag{13}$$

$$\left(\frac{\partial y_{Gj}}{\partial z}\right)_{z=L_R} = \left(\frac{\partial y_{Sj}}{\partial z}\right)_{z=L_R} = \left(\frac{\partial T_G}{\partial z}\right)_{z=L_R} = \left(\frac{\partial T_S}{\partial z}\right)_{z=L_R} = 0 \tag{14}$$

The set of partial differential equations, together with the algebraic equations that provide the transport and reaction properties, has been solved by means of the 'method of lines'. This method, proved to be accurate in previous works [8, 32], consists of approximating the space derivatives by finite differences obtained from Taylor polynomials. All the calculations have been carried out using a code written in MATLAB software. The resulting set of ordinary differential equations (with only one independent variable: time) is solved using the MATLAB function *ode15s*, especially suited to handle stiff problems.

3. Results and discussion

3.1. Experimental study

The main purpose of the experimental study is to determine at which conditions stable reverse-flow operation is possible when using a ceramic foam bed. The experiments have been planned varying the most important operating variables affecting the stability of the reactor: methane inlet concentration (measured in terms of adiabatic temperature rise, 50-150ºC, equivalent to 1800 to 5420 ppm), switching time (50-900 s) and total gas flow rate (15-30

L/min n.t.p.). Experiments have been carried out in the adiabatic bench-scale unit described in the methodology section.

Figure 2 shows pseudo-steady state temperature and concentration profiles for two experiments, operated at 15 L/min (n.t.p.), feed with ΔT_{ad} = 150ºC (5420 ppm methane), and 300 s (Figure 2a) and 600 s (Figure 2b) switching time. The temperature profiles exhibit a parabolic shape, characteristic of reverse-flow reactors, with a high temperature plateau in the middle of the reactor. As this plateau migrates from one side of the bed to the other, the reaction front also moves. It can be observed that switching time has a marked influence in the shape of the temperature profile, the temperature plateau being narrower and moving within a broader range for high switching time. Thus, a higher portion of the bed, and in particular of the zone containing catalyst, cools down, which results in a more pronounced displacement (to the right in this case) of the reaction front in the catalytic bed. The effect of switching time can be also observed in Figure 3a, which shows temperature profiles obtained at the end of the direct half-cycle for ΔT_{ad} 75ºC. On increasing the switching time, the heat stored in the bed, and hence the temperature plateau, decreases. This results in a reactor closer to extinction for switching time 200 s. Figure 3b shows the effect methane feed concentration (ΔT_{ad} 100, 120 and 150ºC). Increasing feed methane concentration increases the heat released in the reaction, and hence the heat stored in the reactor between cycles, producing a higher plateau temperature.

Figure 4 and Figure 5 present experimental results obtained at the following conditions: feed flow rate 15 L/min (n.t.p.), switching time 300 s, and methane concentration corresponding to 100ºC and 150ºC adiabatic temperature rise. These two sets of conditions result in stable (ΔT_{ad} =150ºC) and un-stable (ΔT_{ad}=100ºC) reactor operation. Figure 4 depicts temperature measured at different bed positions as a function of time (given the symmetry of the profiles, only one half of the reactor is represented). Graphs corresponding to ΔT_{ad}=100ºC show a decrease in

the temperature measured by all the thermocouples along the bed, because at these conditions the heat stored in the reactor between cycles is not enough to maintain autothermal operation of the reactor. The outlet methane concentration in this experiment, (Figure 5), is very low (high methane conversion) at the beginning of the experiment (before 25 min), but it starts increasing (conversion decreases) when the temperature in the middle of the reactor lowers close to the ignition temperature. For running time long enough, the reactor temperature will fall below the ignition temperature, and the reactor will extinguish. For the experiment carried out at ΔT_{ad}=150ºC the bed temperature does not decrease continuously, but it evolves until reaching the pseudo-steady state, and outlet methane conversion keeps close to total conversion, because the regenerative heat storage between cycles maintains the long-term reactor stability.

These results indicate that the reactor stability decreases as switching time increases and methane concentration decreases, results qualitatively similar to that for reverse-flow reactors equipped with other types of beds [3, 8]. Results also demonstrate that working in adequate conditions, foam beds can be used as regenerative heat storage, as both temperature and reaction fronts can be maintained within the bed boundaries.

3.2. Model validation

In this section, the reverse-flow reactor experiments are used to validate the model presented in section 2.4. The validation has been carried out by direct comparison between simulation and experimental results, in terms of temperature and methane concentration. No model parameters have been adjusted in order to fit the experimental data.

The validation has been done using all the experiments; Figures 2 to 5 shows the results most representative. Temperature profiles in Figure 2 show that simulations match the

experimental data, the largest deviations being observed at the end of the cycle in the inert bed situated at the left end. This discrepancy can be explained by the working of our experimental device: during the direct cycle (gas flowing from the left to the right), the temperature of the left bed decreases gradually, and the oven that surrounds the reactor tube, responsible of the adiabatic behaviour, must cold down to match the temperature inside the reactor. The oven happens to be slower for cooling down that for heating, and is not able of cooling down as fast as the bed, and as a result, the oven does not behave completely adiabatically, but some heat is transferred from the oven to the reactor.

Temperature profiles such as the ones depicted in Figure 4 have shown to be especially useful to evaluate the performance of simulation models [3, 8]. It can be observed that the model predicts the temperature evolution very well; the mayor discrepancies appearing at the end of every cycle, when the model slightly underestimates temperatures. However, discrepancies are within the error associated to the experimental device.

Experimental and simulated outlet methane concentrations are compared in Figure 5. The model matches the experimental data, even for the un-stable experiment. Experimental data exhibit a peak in methane concentration at every flow switch, caused by the emission of the un-reacted methane present in the inert beds and the piping situated between the reactor and the switch valves produced every time the flow is reversed (phenomenon often referred to in the literature as “wash-out”). The amount of methane emitted this way is very small, except when operating the reverse-flow reactor at very low switching times (less than 50 s).

The general good agreement between model predictions and experimental results, both for stable and un-stable operation, allow considering the simulation model as experimentally validated.

3.3. Reverse-flow reactor bed types: reactor design

One of the decisions taken in the early stages of the design of reverse-flow reactors is the selection of the type of bed. This section is devoted to provide some information useful for the selection of the bed type for a given design problem, by comparing the performance of reverse-flow reactors equipped with three types of beds: random particles, honeycomb monoliths and ceramic foams. Comparison is performed by means of simulations with the model described in the methodology section. The same model differential equations (2)-(5) are valid to simulate the different bed types considered. The differences between beds are due to the different geometrical and physical properties and the different flow pattern, which results in different correlations to calculate the gas to solid heat and mass transport coefficients and the heat and mass axial dispersion, as shown in Table 2.

The model, formed by differential equations and the corresponding correlations, has been validated for ceramic foam beds and at reverse-flow operating conditions in the previous section. The validation for beds of random particles and honeycomb monoliths was presented and discussed in detail in previous works [3, 8, 23].

Comparison of the different bed types is very difficult, as they differ in many properties, including geometry, bulk density, pressure drop, mass and heat transfer, and catalytic characteristics. There are many criteria that can be used for the comparison. As in this case the bed is a catalytic one, and its main function is to convert methane to full oxidation products, the comparison criteria was selected based on the bed catalytic properties.

The catalytic beds are commonly formed by a support material covered by a washcoating layer with better properties as support of the active phase. In the comparison, we have considered that the washcoating layer in the three beds is the same, e.g. it has the same thickness (L_w = 10^{-4} m) and fraction of active phase (2%, wt. Pd/wt. washcoat), providing then the same catalyst activity. The corresponding geometrical properties of the beds have been calculated

so that their specific external surface area (S_v= 1600 m^2/m^3_{bed}) and wall thickness ($5 \cdot 10^{-4}$ m, including the washcoating thickness) are the same, as shown in Table 3. The resulting beds are a foam of 7 ppi with 80% bed porosity, a honeycomb monolith of 200 cpsi with 52% bed porosity and a bed of Raschig rings with 3.16 mm external diameter and 60% bed porosity. In this way, the weight of catalyst active phase (and the intrinsic catalyst activity) per unit volume of bed is the same for the 3 beds compared. The physical properties of the beds, e.g. solid density, heat capacity and thermal conductivity, are the same (see Table 3), as the beds are considered to be made of the same material (in this case a refractory ceramic).

The 3 bed types are compared by designing a reverse-flow reactor for each bed type that operates with the same performance for given conditions. The reactor feed consists of air containing 1000 ppm methane (ΔT_{ad} = 22.7ºC). The design of the reactor involves the calculation of the reactor length and diameter needed for treating a given feed. As the reactor diameter is related to the superficial velocity and total gas flow rate, and the reactor performance depends on the superficial velocity [8, 31], the reverse-flow reactor is designed for different superficial velocities in the range 0.25 – 1.5 m/s (measured at normal conditions). The reactor length is calculated so that 99% stable conversion is achieved when operating with 300 s switching time. As pointed out in the Experimental section, switching time strongly affects the reactor behaviour, and hence the length required to achieve a pre-defined conversion. Thus, very high switching times require very large reactors, and very low switching times reduce the lifetime of the switching valves and increase the wash out effect. The value selected for switching time, 300 s, can be considered as a good balance between these two factors [1, 35]. In the model used, temperature and concentration through the reactor do not depend on the reactor diameter. For this reason, in the calculations it is not necessary to specify feed flow rate or reactor diameter. If one of these two variables is specified, the other can be easily calculated, given the superficial velocity.

The reactor length needed for achieving stable 99% outlet conversion is calculated by simulating the reactor with different bed lengths up to the pseudo-steady state. As an example, Figure 6 shows the results for the case of 0.5 m/s superficial velocity. Each point of the curves corresponds to a single simulation up to the pseudo-steady state. It can be observed that below a characteristic reactor length, conversion falls to zero (reactor extinction occurs).

3.4. Reverse-flow reactor bed types: comparison

Figure 7 to 9 show the results of the reactor design and some properties corresponding to different superficial velocities and for the specifications indicated in the previous section.

The reactor length required to achieve 99% stable conversion (Figure 7a) indicates that on increasing the superficial velocity the reactor length increases. Increasing superficial velocity means increasing the reactor feed per unit bed transverse area, and this would require an increase in space time and reactor length. But in our reverse-flow reactor, the reaction zone does not occupy the whole bed length (see Figure 2), so the increase in reactor length is mainly required to compensate the increase in the speed of the heat wave travelling inside the reactor produced by the increase in superficial velocity. The honeycomb monolith bed requires the lower bed length for all the superficial velocities studied, followed by the foam and random particle beds. The slope of the curve for the foam bed is the smallest, and for the particulate bed the highest, so that for high superficial velocities the performance of the foam gets close to the honeycomb monolith beds, whereas that of the particulate bed is much worse. The observed tendencies can be explained by the influence of the thermal inertia of the bed. Thus, the foam with higher bed porosity than the honeycomb monolith (0.8 and 0.52, respectively) presents lower heat storage capacity (J/m^3_{bed}), so the speed of the heat wave

travelling inside the reactor is higher. For this reason, the foam bed requires a higher length to avoid the hot temperature plateau leaving the reactor.

Figure 7b represents the reactor volume needed for 1 m^3/s (normal conditions) feed flow rate. The performance of all beds improves when increasing the superficial velocity. This is related to the variations of temperature profile and other properties discussed in the next paragraphs. Considering the volume needed to treat a given feed, it is better operating at high flow rates. The best performance corresponds to the honeycomb monolith, followed very close by the foam for superficial velocities higher than 1 m/s. The particulate bed provides the worse performance, except for very low superficial velocity.

Maximum temperatures attained in the temperature plateau in the reactor centre are depicted in Figure 7c as a function of superficial velocity. Maximum temperature in the random particle bed depends very little on the superficial velocity, whereas for the honeycomb monolith bed it increases slightly with superficial velocity, and for the foam bed the increase is very pronounced. This behaviour is explained by the differences in thermal inertia of the beds, $(1-\varepsilon_b)\rho_S C_{PS}$, related to the capacity of the bed to store energy as sensible heat. The foam bed has the lowest bed porosity (80% against 60% and 52% of the random particle and honeycomb monolith beds, respectively), and hence the lower thermal capacity (360 kJ/m^3_{bed} K vs. 720 kJ/m^3_{bed} K and 864 kJ/m^3_{bed} K of the random particle and honeycomb monolith beds, respectively). Since a similar amount of heat must to be stored in the bed every cycle in order to maintain stable operation (for a given heat released by the reaction and switching time), the foam bed, with lower heat storage capacity, produces a higher bed temperature at the pseudo-steady state.

The longer bed required by random particles when compared to the honeycomb monolith bed is not in agreement with results in a previous work [32], and is explained by the lower

temperature plateau, and hence lower reaction rates, attained by the particulate bed, as shown in Figure 7b.

The simulations carried out in this section assume that the reactor is formed by a uniform catalytic bed. But the parabolic temperature profiles characteristic reverse-flow reactors (see Figure 2) mean that at both sides of the high temperature plateau the temperature is too low for the reaction to take place appreciably, and hence, in this part of the bed the catalyst is usually substituted by inert material for economy. The length of the catalytic bed that can be replaced by inert material (considered in this case to be of the same type and properties) can be estimated from the simulated conversion profiles at the pseudo-steady state, as the bed length for which 10% conversion is attained at the end of a direct cycle (gas flowing from the left to the right). Although the substitution of part of the catalytic bed by inert could produce a decrease in outlet conversion, our simulation results indicate that for our conditions, the conversion decrease is very small and within the error of the model predictions.

Figure 8a shows the fraction of the catalytic bed that, according to these results, cannot be substituted by inert material. As shown, this fraction varies only slightly with superficial velocity and is very similar for the random particle and honeycomb monolith beds, in the range 52-57% for all the superficial velocities considered. This is explained by the little influence of the superficial velocity in the plateau temperature, as discussed above. On the other hand, the bed fraction that cannot be substituted by inert material for the foam bed increases from 50 to 70% when increasing superficial velocity, because, due to the low thermal capacity of foams, most of the bed must be catalytic in order to maintain the reaction zone in the catalytic bed for high superficial velocities. Combining the results in Figure 8a with the volume needed for treating 1 m^3/s (n.t.p.) of feed (Figure 7b), one can calculate the volume of catalyst bed, and hence the mass of active phase, needed for every bed type. Results are shown in Figure 8b. The shape of the curves is similar to the ones in Figure 8a, the honeycomb monolith being the

bed that requires less active phase at all conditions studied. The difference between honeycomb monolith and foam is bigger than in Figure 7b, due to the higher fraction of catalytic bed required by foams. The particulate bed requires the higher amount of active phase, except for very low superficial velocity.

Another important characteristic of reverse-flow reactor from an economical point of view is pressure drop. Thus, this variable depends on bed length, shape and geometrical properties of the bed. Figure 8c depicts the pressure drop needed to achieve 99% stable conversion for the 3 beds considered. As expected, the particulate bed presents the higher pressure drop, followed at great distance by the foam and honeycomb monolith beds, in this order. The difference in pressure drop between the bed types increases on increasing the superficial velocity, which means that the use of structured beds, and in particular the honeycomb monolith bed, is favoured at these conditions. It is well known that structured beds (foam and honeycomb monolith) produce lower pressure drops due to the more efficient gas-solid contact and the higher bed porosity, and hence are more adequate for processing high feed flow rates.

Figure 9 compares the different bed types in terms of transport properties, related to the reaction rate and heat transfer, and hence to the performance of reverse-flow reactors. Gas-solid mass and heat transfer coefficients are higher for the foam bed, followed by the particulate and honeycomb monolith beds, in this order (Figure 9a and b). In addition, mass and heat transfer in the foam bed increase substantially with superficial velocity, as the shape of the foam bed favours turbulence on increasing gas velocity. On the contrary, the shape of the honeycomb monolith bed reduces or eliminates turbulence (the flow pattern is laminar), and for this reason the coefficients are unaffected by the superficial velocity.

The axial mass and heat gas dispersion coefficients are depicted in Figure 9c and d. Superficial velocity increases axial dispersion for all bed types, as a consequence of the increase of

turbulence in the fluid phase. The foam bed presents considerably higher axial dispersion coefficients, as it produces the higher turbulence. High mass axial dispersion coefficients can be negative for the reactor performance, as they produce deviation from plug flow and decrease conversion, but in this case values of the dispersion modulus D_{ez}/u_0L_R for the foam bed are very low (always lower than $3 \cdot 10^{-2}$), so in our conditions axial dispersion has no practical negative effect on the reactor performance.

Gas heat axial dispersion favours heat transmission in the axial coordinate. It depends on the convective heat transfer, connected to gas axial mixing, the gas-solid heat transfer coefficient and the solid effective thermal conductivity. Very low axial heat dispersion may produce hot spots in the bed temperature profiles, which can be difficult to dissipate and can cause local catalyst thermal deactivation, but very high axial heat dispersion can produce too much axial heat transfer from the hot bed centre to the colder bed sides, which would reduce the thermal efficiency of the regenerative heat transfer between the hot gas and the bed that must take place in the bed ends. Then, if using a solid with low thermal conductivity (typically less than 0.5 W/m K) as catalyst support, it would be interesting shaping this material as foam bed, in order to favour axial heat dispersion in the gas phase. For solids with higher thermal conductivity, as in our case, the axial heat transfer in the solid phase is enough to avoid hot spots, and axial gas mixing, and hence, the type of bed is of little relevance for the axial heat transfer.

4. Conclusions

Experiments performed in a bench-scale adiabatic reverse-flow reactor equipped with a ceramic foam catalytic bed have demonstrated that despite the low thermal inertia of the ceramic foam, the stable reverse-flow operation was possible for the catalytic combustion of

lean methane-air mixtures. The results indicate that the reactor stability decreases as switching time increases and methane concentration decreases, results qualitatively similar to that for reverse-flow reactors equipped with other types of beds. Thus, the switching time plays a similar role as in other reverse-flow reactors, controlling the amount of heat stored in the bed between cycles and hence the maximum bed temperature and reactor stability.

A detailed mathematical model, formed by the conservation equations (mass and energy balances) and specific correlations used to calculate the physical and transport properties of a foam bed, has been proposed to simulate the behaviour of reverse-flow reactors equipped with ceramic foam beds. The model has been validated by direct comparison of the simulations with the experiments, concluding that the model can predict with high accuracy the experimental results.

The model has been used to design reverse-flow reactors containing different types of beds: ceramic foam, Raschig ring and a honeycomb monolith. The comparison of beds of equivalent geometry showed that for the conditions studied the honeycomb monolith bed is the more efficient. It requires the lower bed length and active phase mass, and produces the lower pressure drop. The foam bed was found to present better gas to solid transport properties (both mass and heat) and a competitive pressure drop, while being less efficient than the honeycomb monolith for heat storage. For this reason, the use of foam beds is favoured in the catalytic bed of the centre of the reactor, where fast mass and heat transfer is demanded, whereas the honeycomb monolith should be used in the inert beds, where high heat storage capacity is preferred.

Acknowledgements

SICAT is gratefully acknowledged for supplying the foams supports. This work was supported by the Research Fund for Coal and Steel of the European Union (contract UE-10-RFCR-CT-2010-

00004). The author Claire R. Thomson acknowledges the financial support of the Erasmus Program (University of Oviedo-Strathclyde University, Glasgow).

Nomenclature

Latin symbols

a	foam window or pore diameter (m)
a_G	S_v/ϵ_b, geometric surface area per unit of gas volume (m^2/m^3_{gas})
a_S	$S_v/(1-\epsilon_b)$, geometric surface area per unit of solid volume (m^2/m^3_{solid})
c	total molar concentration (mol/m^3)
C_P	heat capacity (J/kg K)
d	characteristic length, d_P for random particle, d_h for honeycomb monoliths and $\frac{3}{2}d_s$ for foams (m)
d_h	$4/a_G$, hydraulic diameter (m)
d_s	strut length (m)
Da	$\lvert r_m \rvert \eta_j \rho_S D_h / a_S D_{jm} y_g c_g$, Damkoeler number
D_{ep}	effective pore diffusion coefficient (m^2/s)
D_{ez}	effective axial dispersion coefficient (m^2/s)
D_{jm}	molecular diffusion coefficient of *j* in the mixture (m^2/s)
d_{pore}	catalyst mean pore size (m)
E_a	activation energy (J/mol)
f_{cat}	catalytic bed fraction (m_{cat}/m_{tot})
f_w	volume fraction of washcoating ($m^3_{washcoating}/m^3_{solid}$)
G	$2\sqrt{(1-\epsilon_b)/3\pi}$, function of the foam empty volume fraction
h_G	gas to solid heat transfer coefficient (W/m^2 K)
k_G	thermal conductivity (W/m K)
k_{Gez}	effective axial thermal dispersion coefficient (W/m K)

K_G	gas to solid mass transfer coefficient (m/s)
k_m	kinetic constant per unit of catalyst mass (mol/kg_{cat} s Pa)
k_0	pre-exponential factor (mol/kg_{cat} s Pa)
L	length (m)
M_{Pd}	Weight of Pd active phase (kg)
Nu	$h_G d/k_g$, Nusselt number
p	pressure (Pa)
Pe^H	$d_h v \rho_G C_{PG}/k_G$, Peclet number for heat transfer
Pe^M	$d_h v/D_{jm}$, Peclet number for mass transfer
PE_{ax}^H	$d_h v \rho_G C_{PG}/\kappa_{G,ax}$, Peclet number for axial heat dispersion
PE_{ax}^M	$d_h v/D_{j,ax}$, Peclet number for axial mass dispersion
Pr	$C_{PG}\mu_G/\kappa_G$, Prandlt number
$(r_j)_m$	reaction rate of *j* per unit weight of catalyst (mol/kg_{cat} s)
R_g	ideal gas constant (8.314 J/mol K)
Re	$d\ v_0 \rho_{G0}/\epsilon_b \mu_G$, Reynolds number
Sc_j	$\mu_G/\rho_G D_{jm}$, Schmidt number
Sh_j	$K_G\ d/D_{jm}$, Sherwood number
S_v	geometric surface area per unit of bed volume (m^2/m^3_{bed})
T	temperature (K)
v	interstitial velocity (m/s)
V_R	reactor volume (m^3)
X	conversion
y	molar fraction

z	axial coordinate (m)
z^*	$z/d_h Pe$, dimensionless axial coordinate

Subscripts

0	inlet conditions
ax	axial
b	bed
G	gas
H	constant heat flux
int	internal
j	*j*-compound
m	mixture/mass
R	reactor
S	solid
T	constant temperature

Superscripts

H	heat
M	mass

Greek symbols

ϵ	porosity, -
ΔH_j	combustion enthalpy of *j* (J/mol)
ϕ	Thiele modulus
η	intenal effectiveness factor
μ	viscosity (kg/m s)
ρ	density (kg/m^3)

τ	tortuosity

Caption to figures

Figure 1 Photograph of a foam cell obtained with a stereo microscope, indicating the measurement of cell size (ϕ), pore size (a), and strut diameter (d_s).

Figure 2 Temperature and concentration profiles of the foam reverse-flow reactor at the beginning (o …), the middle (Δ --), and the end (□ ▬) of the half cycle starting at 40 min. Flow direction from left to right. Symbols: experiments. Lines: simulations.
Q_G = 15 L/min at n.t.p. ΔT_{ad} = 150ºC. t_{sw} = 300 s (a and c) and 600 s (b and d).

Figure 3 Foam reverse-flow reactor temperature profiles at different methane feed concentrations (a) and switching times (b). End of half cycle with flow direction from left to right. Q_G = 15 L/min at n.t.p.
(a) t_{sw} = 300 s. ΔT_{ad} = 100 (◊),120 (Δ) and 150ºC (o).
(b) ΔT_{ad} = 75ºC. t_{sw} = 50 (o), 100 (Δ) and 200 (◊) s.

Figure 4 Comparison of experiments (▬) and model predictions (▬): evolution of bed temperature with time. Q_G = 15 L/min at n.t.p. t_{sw} = 300 s. ΔT_{ad} = 100 (a) and 150ºC (b).

Figure 5 Comparison of experiments (▬) and model predictions (▬): evolution of methane outlet concentration with time. Q_G = 15 L/min at n.t.p. t_{sw} = 300 s. ΔT_{ad} = 100 (a) and 150ºC (b).

Figure 6 Major conversion as a function of bed length for the random particle (o), honeycomb monolith (□) and foam (◊) reverse-flow reactors. u_0 = 0.5 m/s (n.t.p.), t_{sw} = 300 s, y_{G0} = 1000 ppm (ΔT_{ad} = 27.7ºC).

Figure 7 Comparison of random particle (o), honeycomb monolith (□) and foam (◊) reverse-flow reactors at different gas flow velocities: (a) reactor length required for 99% conversion, (b) reactor volume corresponding to feed 1 m^3/s (n.t.p.), and (c) maximum solid temperature.

Figure 8 Comparison of random particle (o), honeycomb monolith (□) and foam (◊) reverse-flow reactors at different gas flow velocities: (a) catalyst bed fraction, (b) mass of active phase contained for feed 1 m^3/s (n.t.p.), and (c) total pressure drop.

Figure 9 Comparison of random particle (o), honeycomb monolith (□) and foam (◊) reverse-flow reactors at different gas flow velocities: (a) gas-solid mass transfer coefficient, (b) gas-solid heat transfer coefficient, (c) mass axial dispersion coefficient, and (d) effective axial thermal conductivity.

Figure 1

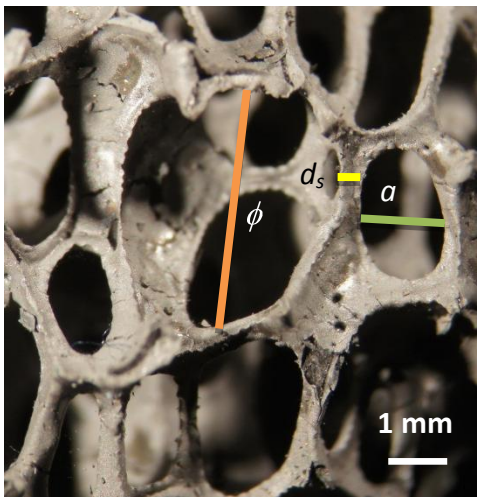

Figure 2

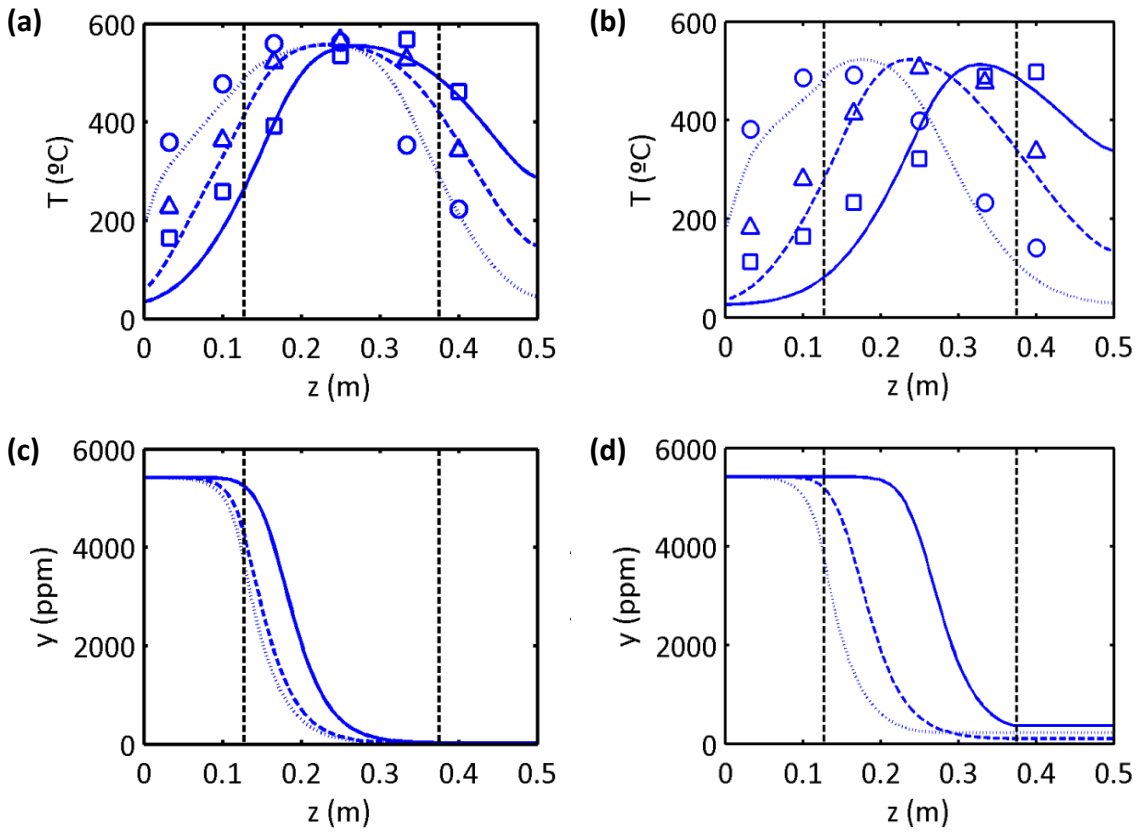

Figure 3

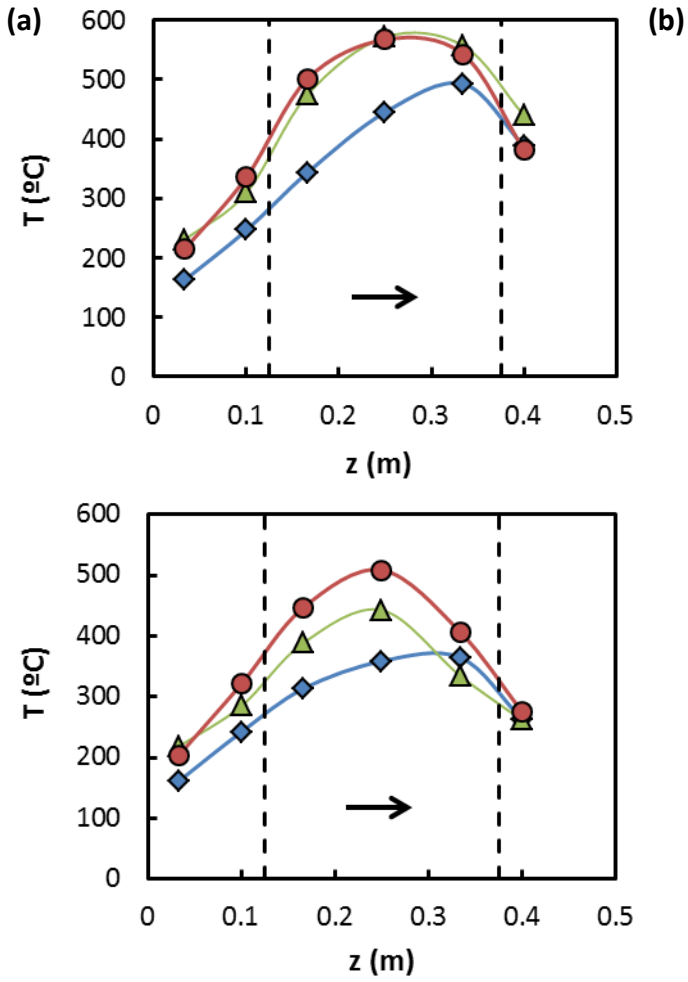

Figure 4

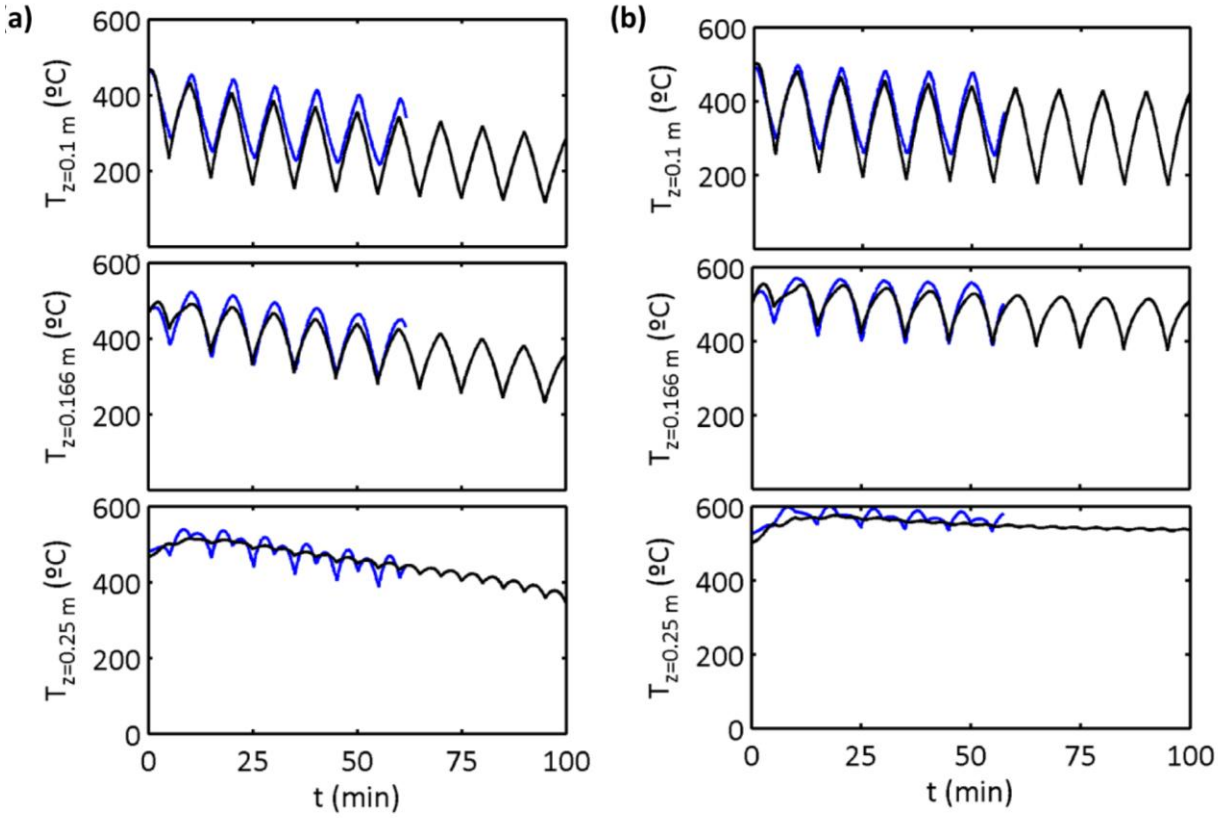
(a)
(b)
600
400
200
0
$T_{z=0.1\ m}$ (ºC)
$T_{z=0.166\ m}$ (ºC)
$T_{z=0.25\ m}$ (ºC)
0
25
50
75
100
t (min)

Figure 5

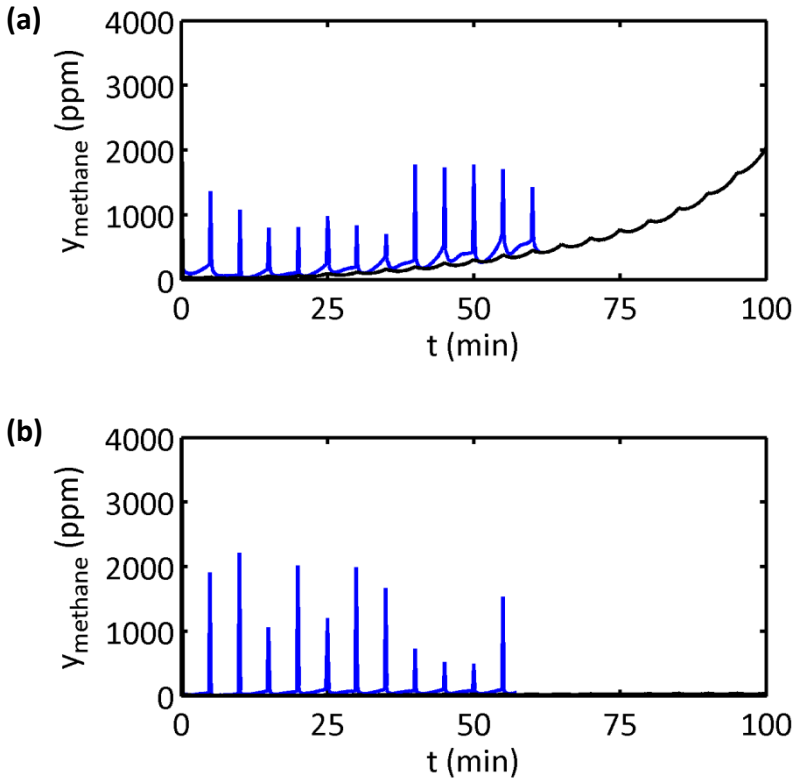
(a)
4000
3000
2000
1000
0
$y_{methane}$ (ppm)
0
25
50
75
100
t (min)
(b)
4000
3000
2000
1000
0
$y_{methane}$ (ppm)
0
25
50
75
100
t (min)

Figure 6

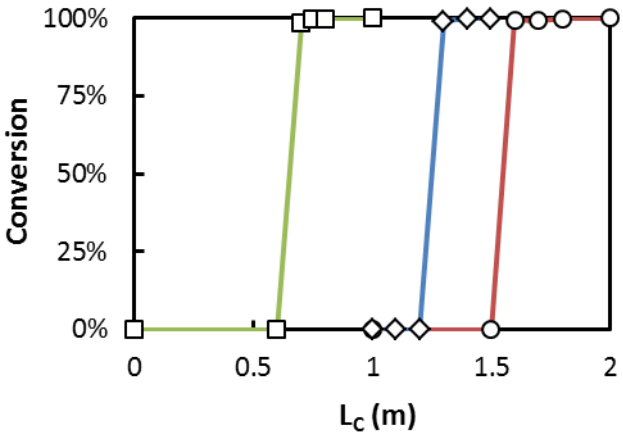

Figure 7

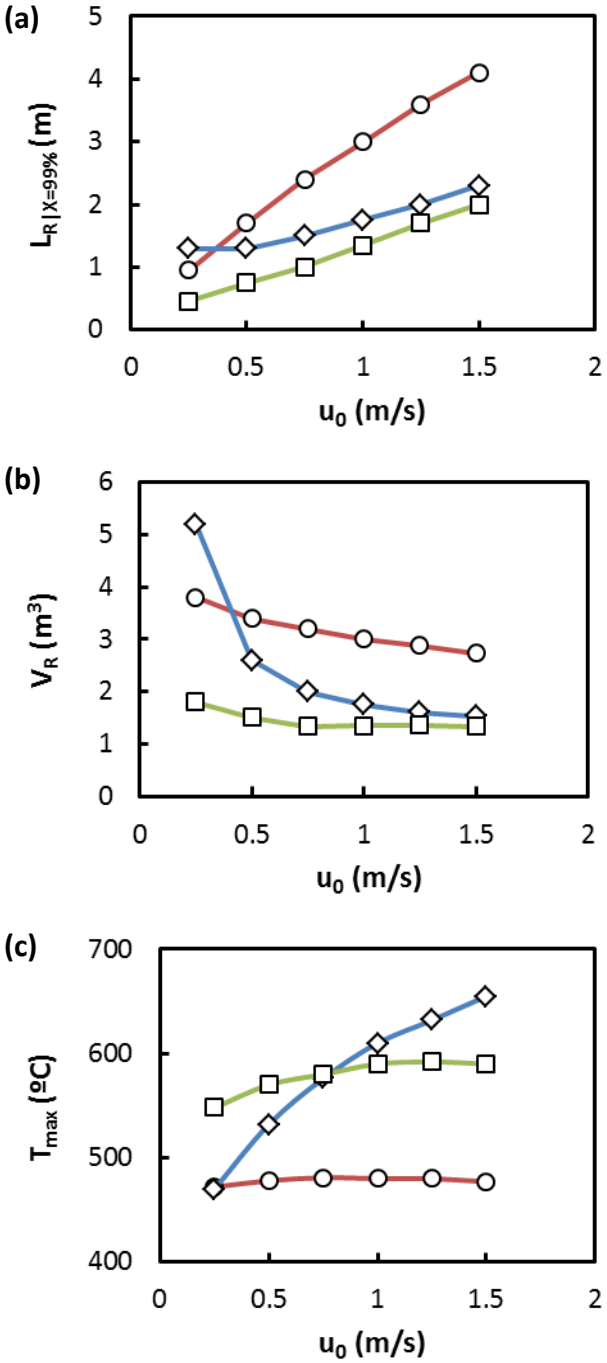

Figure 8

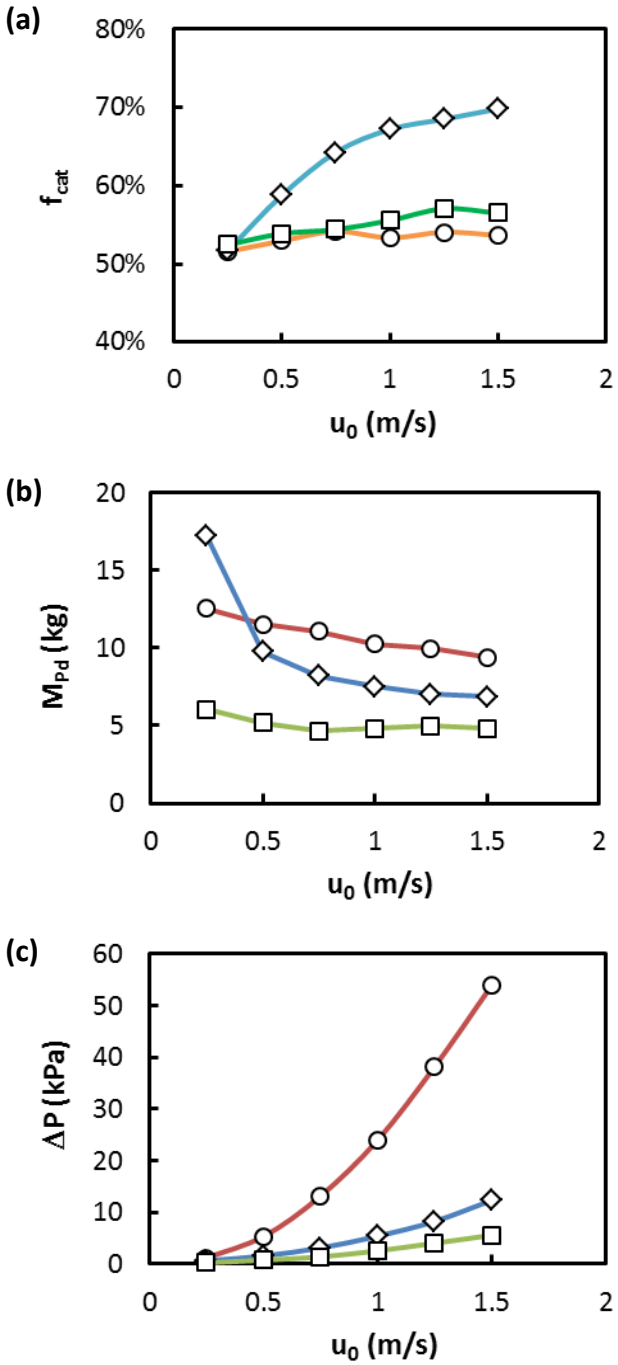
(a)
80%
70%
60%
50%
40%
f_{cat}
0
0.5
1
1.5
2
u_0 (m/s)
(b)
20
15
10
5
0
M_{Pd} (kg)
0
0.5
1
1.5
2
u_0 (m/s)
(c)
60
50
40
30
20
10
0
ΔP (kPa)
0
0.5
1
1.5
2
u_0 (m/s)

Figure 9

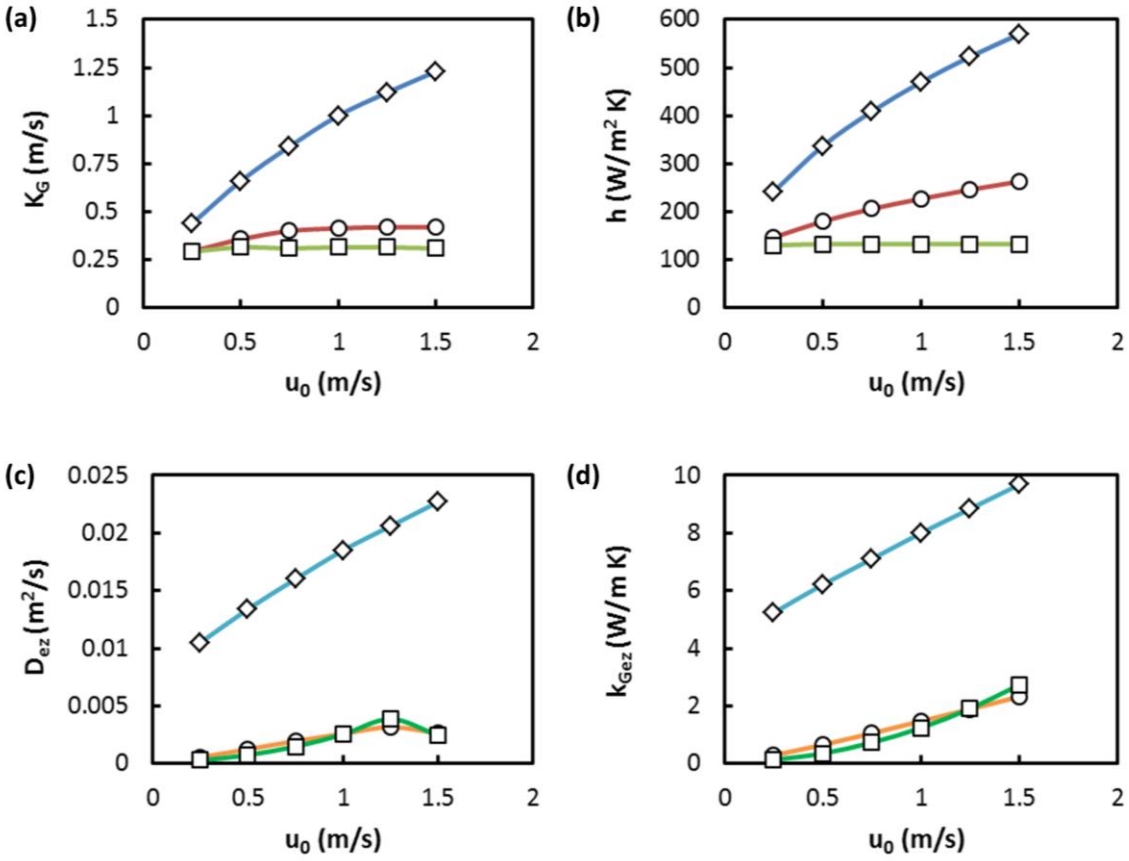
(a)
K_G (m/s)
1.5
1.25
1
0.75
0.5
0.25
0
0
0.5
1
1.5
2
u_0 (m/s)
(b)
h (W/m^2 K)
600
500
400
300
200
100
0
0
0.5
1
1.5
2
u_0 (m/s)
(c)
D_{ez} (m^2/s)
0.025
0.02
0.015
0.01
0.005
0
0
0.5
1
1.5
2
u_0 (m/s)
(d)
k_{Gez} (W/m K)
10
8
6
4
2
0
0
0.5
1
1.5
2
u_0 (m/s)

List of tables

Table 1

Geometrical properties	
Pore density	7 ppi
Cell size, ϕ	$3.54 \cdot 10^{-3}$ m
Pore size, a	$1.15 \cdot 10^{-3}$ m
Strut diameter, d_s	$4.7 \cdot 10^{-4}$ m
Bed porosity, ϵ_b	0.8
Specific external surface area, S_v	1700 m^2/m^3_{bed}
Mean pore size, d_{pore}	$2.77 \cdot 10^{-8}$ m
Internal porosity, ϵ_{int}	0.27
Internal tortuosity, τ_{int}	4
Physical properties	
Apparent density, ρ_b	220 kg/m^3
Solid density, ρ_S	2670 kg/m^3
Solid heat capacity, C_{PS}	348 + 125 ln $(T - 273)$ J/kg K
Solid thermal conductivity, k_S	8.1 W/m K
Intrinsic reaction properties	
Pre-exponential factor, k_0	15 mol/kg_{cat} s Pa
Activation energy, E_a	89 kJ/mol
Enthalpy of combustion, ΔH_{CH_4}	- 802.5 kJ/mol

Table 2

Random particle bed		Honeycomb monolith bed		Foam bed	
Gas to solid transport					
$Sh = 2 + f_{TM} Re^{1/2} Sc^{1/3}$	[23]	$Sh_H = 3.095 + 8.933(1000z^*)^{-0.5386} \exp(-6.7275z^*)$ $Sh_T = 2.977 + 6.854(1000z^*)^{-0.5174} \exp(-42.49z^*)$ $\frac{Sh - Sh_H}{Sh_T - Sh_H} = \frac{Da\, Sh}{(Da + Sh)Sh_T}$	[35]	$Sh = 0.91\ (Re_{max})^{0.43}\ Sc^{1/3}$	[33]
$Nu = 2 + f_{TC} Re^{1/2} Pr^{1/3}$	[23]	$Nu_H = 3.095 + 8.933(1000z^*)^{-0.5386} \exp(-6.7275z^*)$ $Nu_T = 2.977 + 6.854(1000z^*)^{-0.5174} \exp(-42.49z^*)$ $\frac{Nu - Nu_H}{Nu_T - Nu_H} = \frac{Da\, Nu}{(Da + Nu)Nu_T}$	[35]	$Nu = 1.0\ (Re_{max})^{0.43}\ Pr^{1/3}$	[33]
Axial dispersion					
$D_{ax} = \left(\frac{d_P v_0 \rho_{G0}}{\rho_G}\right)\left[\frac{0.73}{Re\, Sc} + \frac{0.5}{1 + \frac{9.7}{Re\, Sc}}\right]$	[23]	$PE_{ax}^M = \left[\frac{1}{Pe^M} + \frac{Pe^M}{192}\right]^{-1}$		$PE_{ax}^M = \left[\frac{87}{Pe^M} + 0.84\right]^{-1}$	[34]
$\kappa_{G,ax} = (d_P v_0 \rho_{G0} C_{PG})\left[\frac{0.73}{Re\, Pr} + \frac{0.5}{1 + \frac{9.7}{Re\, Pr}}\right]$	[23]	$PE_{ax}^H = \left[\frac{1}{Pe^H} + \frac{Pe^H}{192}\right]^{-1}$		$PE_{ax}^H = \left[\frac{87}{Pe^H} + 0.84\right]^{-1}$	[34]
Friction factor					
$f = \frac{2(1-\epsilon_b)}{\epsilon_b^3}\left(\frac{150}{Re_p} + \frac{4.2}{Re_p^{1/6}}\right)$		$f = \left(\frac{4}{\epsilon_b^2}\right)\frac{13.3}{Re}$		$f = 2\left(\frac{1-\epsilon_b}{\epsilon_b^3}\right)\left(\frac{150}{Re} + \frac{4.2}{Re^{1/6}}\right)$	[7]

Table 3

Common properties	
Specific external surface area, S_v	1600 m^2/m^3_{bed}
Washcoating thickness, L_w	10^{-4} m
Wall thickness	$5 \cdot 10^{-4}$ m
Solid density, ρ_S	2000 kg/m^3
Solid heat capacity, C_{PS}	900 J/kg K
Solid thermal conductivity, k_S	1 W/m K
Raschig rings	
External particle diameter	$3.16 \cdot 10^{-3}$ m
Internal particle diameter	$2.16 \cdot 10^{-3}$ m
Height of particle	$3.16 \cdot 10^{-3}$ m
Sphere equivalent diameter, d_{esf}	$2.93 \cdot 10^{-3}$ m
Sphericity	0.51
Equivalent particle size, d_P	$1.5 \cdot 10^{-3}$ m
Bed porosity, ϵ_b	0.6
Washcoating fraction , f_w	0.4
Honeycomb monolith	
Cell density	200 cpsi
Hydraulic diameter, D_h	$1.31 \cdot 10^{-3}$ m
Bed porosity, ϵ_b	0.52
Washcoating fraction, f_w	0.34
Foam	
Pore density	7 ppi
Cell size, ϕ	$3.54 \cdot 10^{-3}$ m
Pore size, a	$1.15 \cdot 10^{-3}$ m
Strut diameter, d_s	$5 \cdot 10^{-4}$ m
Bed porosity, ϵ_b	0.8
Washcoat fraction, f_w	0.8

References

[1] A.A. Barresi, G. Baldi, D. Fissore, Forced unsteady-state reactors as efficient devices for integrated processes: Case histories and new perspectives, Industrial & Engineering Chemistry Research, 46 (2007) 8693-8700.

[2] Y.S. Matros, G.A. Bunimovich, Reverse-Flow Operation in Fixed Bed Catalytic Reactors, Catalysis Reviews, 38 (1996) 1 - 68.

[3] P. Marin, S. Ordonez, F.V. Diez, Combustion of toluene-hexane binary mixtures in a reverse flow catalytic reactor, Chemical Engineering Science, 63 (2008) 5003-5009.

[4] S. Su, J. Agnew, Catalytic combustion of coal mine ventilation air methane, Fuel, 85 (2006) 1201-1210.

[5] P. Marín, M.A.G. Hevia, S. Ordóñez, F.V. Díez, Combustion of methane lean mixtures in reverse flow reactors: Comparison between packed and structured catalyst beds, Catalysis Today, 105 (2005) 701-708.

[6] M.V. Twigg, J.T. Richardson, Theory and Applications of Ceramic Foam Catalysts, Chemical Engineering Research and Design, 80 (2002) 183-189.

[7] M. Lacroix, P. Nguyen, D. Schweich, C. Pham Huu, S. Savin-Poncet, D. Edouard, Pressure drop measurements and modeling on SiC foams, Chemical Engineering Science, 62 (2007) 3259-3267.

[8] P. Marín, S. Ordóñez, F.V. Díez, Monoliths as suitable catalysts for reverse-flow combustors: modeling and experimental validation., AIChE Journal, 56 (2010) 3162-3173.

[9] Z. Taslicukur, C. Balaban, N. Kuskonmaz, Production of ceramic foam filters for molten metal filtration using expanded polystyrene, Journal of the European Ceramic Society, 27 (2007) 637-640.

[10] V.R. Vedula, D.J. Green, J.R. Hellmann, Thermal fatigue resistance of open cell ceramic foams, Journal of the European Ceramic Society, 18 (1998) 2073-2080.

[11] L.S. Escandón, S. Ordóñez, A. Vega, F.V. Diez, Oxidation of methane over palladium catalysts: effect of the support, Chemosphere, 58 (2005) 9-17.

[12] P. Nguyen, C. Pham, Innovative porous SiC-based materials: From nanoscopic understandings to tunable carriers serving catalytic needs, Applied Catalysis A: General, 391 (2011) 443-454.

[13] D. Edouard, M. Lacroix, C.P. Huu, F. Luck, Pressure drop modeling on SOLID foam: State-of-the art correlation, Chemical Engineering Journal, 144 (2008) 299-311.

[14] B. Dietrich, G. Schell, E.C. Bucharsky, R. Oberacker, M.J. Hoffmann, W. Schabel, M. Kind, H. Martin, Determination of the thermal properties of ceramic sponges, International Journal of Heat and Mass Transfer, 53 (2010) 198-205.

[15] G. Incera Garrido, F.C. Patcas, S. Lang, B. Kraushaar-Czarnetzki, Mass transfer and pressure drop in ceramic foams: A description for different pore sizes and porosities, Chemical Engineering Science, 63 (2008) 5202-5217.

[16] Y. Peng, J.T. Richardson, Properties of ceramic foam catalyst supports: one-dimensional and two-dimensional heat transfer correlations, Applied Catalysis A: General, 266 (2004) 235-244.

[17] J.T. Richardson, D. Remue, J.K. Hung, Properties of ceramic foam catalyst supports: mass and heat transfer, Applied Catalysis A: General, 250 (2003) 319-329.

[18] O. Sanz, F. Javier Echave, M. Sánchez, A. Monzón, M. Montes, Aluminium foams as structured supports for volatile organic compounds (VOCs) oxidation, Applied Catalysis A: General, 340 (2008) 125-132.

[19] F.C. Patcas, G.I. Garrido, B. Kraushaar-Czarnetzki, CO oxidation over structured carriers: A comparison of ceramic foams, honeycombs and beads, Chemical Engineering Science, 62 (2007) 3984-3990.

[20] P. Chin, X. Sun, G.W. Roberts, J.J. Spivey, Preferential oxidation of carbon monoxide with iron-promoted platinum catalysts supported on metal foams, Applied Catalysis A: General, 302 (2006) 22-31.

[21] I. Cerri, G. Saracco, V. Specchia, Methane combustion over low-emission catalytic foam burners, Catalysis Today, 60 (2000) 21-32.

[22] C.-H. Zheng, L.-M. Cheng, T. Li, Z.-Y. Luo, K.-F. Cen, Filtration combustion characteristics of low calorific gas in SiC foams, Fuel, 89 (2010) 2331-2337.

[23] D. Fissore, A.A. Barresi, G. Baldi, M.A.G. Hevia, S. Ordóñez, F.V. Díez, Design and testing of small-scale unsteady-state afterburners and reactors, AIChE Journal, 51 (2005) 1654-1664.

[24] G. Eigenberger, G. Kolios, U. Nieken, Thermal pattern formation and process intensification in chemical reaction engineering, Chemical Engineering Science, 62 (2007) 4825-4841.

[25] S. Salomons, R.E. Hayes, M. Poirier, H. Sapoundjiev, Flow reversal reactor for the catalytic combustion of lean methane mixtures, Catalysis Today, 83 (2003) 59-69.

[26] U. Nieken, G. Kolios, G. Eigenberger, Fixed-bed reactors with periodic-flow reversal - Experimental results for catalytic combustion, Catalysis Today, 20 (1994) 335-350.

[27] P. Marín, S. Ordóñez, F.V. Díez, Performance of silicon-carbide foams as supports for Pd-based methane combustion catalysts, Journal of Chemical Technology & Biotechnology, 87 (2012) 360-367.

[28] T.V. Choudhary, S. Banerjee, V.R. Choudhary, Catalysts for combustion of methane and lower alkanes, Applied Catalysis A: General 234 (2002) 1-23.

[29] T.T. Huu, M. Lacroix, C. Pham Huu, D. Schweich, D. Edouard, Towards a more realistic modeling of solid foam: Use of the pentagonal dodecahedron geometry, Chemical Engineering Science, 64 (2009) 5131-5142.

[30] P. Marín, S. Ordóñez, F.V. Díez, Rational design of heating elements using CFD: Application to a bench-scale adiabatic reactor, Computers & Chemical Engineering, 35 (2011) 2326-2333.

[31] P. Marin, S. Ordóñez, F.V. Diez, Simplified design methods of reverse flow catalytic combustors for the treatment of lean hydrocarbon-air mixtures, Chemical Engineering and Processing, 48 (2009) 229-238.

[32] M.A.G. Hevia, S. Ordóñez, F.V. Díez, Design and testing of a control system for reverse flow catalytic afterburners, AIChE Journal, 51 (2005) 3020-3027.

[33] G. Groppi, L. Giani, E. Tronconi, Generalized Correlation for Gas/Solid Mass-Transfer Coefficients in Metallic and Ceramic Foams, Industrial & Engineering Chemistry Research, 46 (2007) 3955-3958.

[34] B. Dietrich, M. Kind, H. Martin, Axial two-phase thermal conductivity of ceramic sponges - Experimental results and correlation, International Journal of Heat and Mass Transfer, 54 (2011) 2276-2282.

[35] G. Groppi, A. Belloli, E. Tronconi, P. Forzatti, A comparison of lumped and distributed models of monolith catalytic combustors, Chemical Engineering Science, 50 (1995) 2705-2715.